Crystal characterization and optical spectroscopy of Eu^{3+}-doped $CaGdAlO_4$ single crystal fabricated by the floating zone method

Ruijuan Li (李瑞娟)[1,2], Xiaodong Xu (徐晓东)[3,*], Liangbi Su (苏良碧)[2], Qinglin Sai (赛青林)[4], Changtai Xia (夏长泰)[4], Qiuhong Yang (杨秋红)[1], Jun Xu (徐 军)[5], Adam Strzęp[6], and Anita Półkoszek[6]

[1]*School of Materials Science and Engineering, Shanghai University, Shanghai 200444, China*
[2]*Shagnhai Institute of Ceramics, Chinese Academy of Science, Shanghai 201899, China*
[3]*Jiangsu Key Laboratory of Advanced Laser Materials and Devices, School of Physics and Electronic Engineering, Jiangsu Normal University, Xuzhou 221116, China*
[4]*Shanghai Institute of Optics and Fine Mechanics, Chinese Academy of Science, Shanghai 201800, China*
[5]*School of Physics Science and Engineering, Institute for Advanced Study, Tongji University, Shanghai 200092, China*
[6]*Institute of Low Temperature and Structure Research PAS. Okolna 2 Street, Wroclaw 50-422, Poland*
**Corresponding author: xdxu79@mail.sic.ac.cn*

Received October 15, 2015; accepted November 26, 2015; posted online February 2, 2016

A highly transparent Eu^{3+}-doped $CaGdAlO_4$ (CGA) single crystal is grown by the floating zone method. The segregation coefficient, x ray diffraction, and x ray rocking curve are detected, and the results reveal that the single crystal is of high quality. The *f*–*f* transitions of Eu^{3+} in the host lattice are discussed. The $^5D_0$–$^7F_2$ emission transition at 621 nm (red light) is dominant over the $^5D_0$–$^7F_1$ emission transitions at 591 and 599 nm (orange light), agreeing well with the random crystal environment of Eu^{3+} ions in a CGA crystal. The decay time of Eu:$^5D_0$ is measured to be 1.02 ms. All the results show that the Eu:CGA crystal has good optical characterization and promises to be an excellent red- fluorescence material.

OCIS codes: 160.2540, 300.6170, 260.1180, 160.4670.
doi: 10.3788/COL201614.021602.

Nowadays, white light-emitting diodes (W-LEDs), due to their compact size, eco-friendliness, high brightness, low energy consumption, and long lifetime, are regarded as a viable substitute for traditional incandescent lamps and fluorescent lamps[1]. At present, the most popular W-LED device is phosphor-converted white LEDs[2,3]. However, the phosphor of W-LEDs still has many drawbacks, such as large light decline, poor uniformity, deficiency of red emission[4], a short lifetime, and poor physical and chemical characteristics, which is unfavorable for the performance of the W-LED[1]. Recently, some researchers devoted their attention to the fields of non rare earth (non-RE) such as Bi ion-doped phosphors[5–7] to solve the problems above, and have made great progress in the light decline and deficiency of red emission. However, there are still more problems than a single crystal can solve[8]. Therefore, it is urgently required to seek more stable single crystals to act as substitutes for the red fluorescent materials.

Europium ions have attracted a great deal of attention for their wide use in the field of display and illumination since 1960s. As one of the most frequently used red-emitting activators, the Eu^{3+} ion mainly shows characteristic emissions with high intensity from the transitions of $^5D_0$–^7F_J ($J = 0$, 1, 2, 3, 4, 5, 6)[9,10], and has a long fluorescent lifetime[11].

CGA single crystals have a perovskite structure that belongs to the family of $ABCO_4$ compounds, where A = Ca, Sr, or Ba, $B = a$ rare-earth element, and C = Ga, Al, or a transition element[12,13]. The crystal's structure is a three-dimensional net composed of connected AlO_6 octahedra. A and B ions occupy the same site with a site occupancy factor equal to 0.5. These ions are coordinated by nine oxygen ions[14,15]. Therefore, the dopant ions are distributed in a disorderly manner in the CGA single crystal and occupy the sites without or deviated from inversion symmetry[2]. Due to the high thermal conductivity (6.9 $Wm^{-1}K^{-1}$ along the *a*-axis and 6.3 $Wm^{-1}K^{-1}$ along the *c*-axis), favorable thermal expansion coefficient (10.1×10^{-6} and 16.2×10^{-6} K^{-1} along the *a*- and *c*-axes, respectively), and high mechanical strength (Mohs hardness 6), lanthanide-doped CGA crystals are good candidates for fluorescent and laser materials[16,17]. To date, all of the reported results concerning Ln-doped CGAs are focused on the spectroscopic properties of IR-relevant Ln^{3+} ions such as Nd^{3+}, Er^{3+}, Tm^{3+}, and Yb^{3+}[18–21]. Therefore, in this Letter, we present a report concerning the spectroscopic properties of Eu^{3+}-doped CGA single crystals.

CGA single crystals can be grown by the Czochralski (CZ) method. Due to the strong thermal expansion anisotropy, the crystal growth process is nontrivial, and the obtained boules often posses cleavages parallel to the (001) crystallographic plane[22]. However, the floating zone (FZ) method possesses some advantages over the CZ

method in the growth of these sorts of materials. FZ is much faster and cheaper due to the lack of expensive crucibles. Moreover, the several-millimeter-diameter crystals grown by the FZ method possess a rod-like shape and are thought to have potential as a material for miniature optical device applications because light can pass through the cylindrical crystal without complicated processing[23].

In this Letter, we present the results of different investigations carried on Eu^{3+}-doped CGA single crystals grown by the FZ method. The x ray diffraction (XRD), rocking curve, segregation coefficient, and spectra properties of the Eu:CGA crystal were studied.

A $CaGdAlO_4$ single crystal doped with Eu^{3+} (2 at. %) was grown by the FZ technique. The starting materials were $CaCO_3$, Gd_2O_3, Al_2O_3, and Eu_2O_3 with 5 N purity. They were mixed with stoichiometric proportions. Afterwards, anhydrous ethanol was added, and the obtained slurry was well ground in a ball mill. The mixed powder was dried and pressed into rods (~130 mm long, 10 mm in diameter) by a cold isostatic press (applied pressure: 200 MPa, pressing time: 2 min). The obtained rods were sintered at 1250°C for 20 h for decarbonation in air. Single-crystal growth was carried out in an optical floating-zone furnace (IRF01-001-00, Quantum Design Corporation, America). A CGA single crystal bar (4 mm × 4 mm × 50 mm) oriented in the ⟨100⟩ direction was used as a seed. The sintered rods were rotated at 10 rpm, and the single crystal was grown at a speed of 3–4.5 mm/h in the air atmosphere. Moreover, in order to assure the uniform composition of the molten zone, an opposite rotation at the same rotation speed is necessary[24].

Long and geometrically homogeneous textured cylindrical rods have been obtained [see Fig. 1(a)]. The rod was cut along the (001) plane into ~1 mm thick slices, as shown in Fig. 1(b). As shown in Fig. 1(a), the Eu:CGA single crystal is transparent and slightly brown in color. Color is relevant to the colored centers, which are related to the oxygen vacancies in the crystal structure. Therefore, the piece was annealed in H_2 for 20 h at 1250°C to eliminate the colored center. As shown in Fig. 1(b), the right piece, which was transparent, was annealed in H_2, compared to the left, which is an as-grown crystal.

The crystal structure of Eu:CGA was analyzed by XRD using Cu K_α radiation (D8-Advance, Bruker, Germany). Data was recorded over a range of 10°–70° with a 0.02° step. The rocking curve for the crystal was measured by a high resolution x ray diffractometer (D8-Discover, Bruker, Germany). The segregation coefficient of the Eu^{3+} ion in the CGA crystal was measured by an inductively coupled plasma atomic emission spectrometer (ICP-AES). The absorption spectra were measured by a Cary 5 E Varian spectrophotometer. The emission spectra were measured by exploiting a DongWoo Optron DM750 monochromator coupled to an R-928 Hamamatsu photomultiplier. The luminescence decay kinetics were measured with the use of a Coherent Inc. Libra femtosecond laser coupled with a light conversion OPerA optical parametric amplifier (OPA) as an excitation source and a Princeton

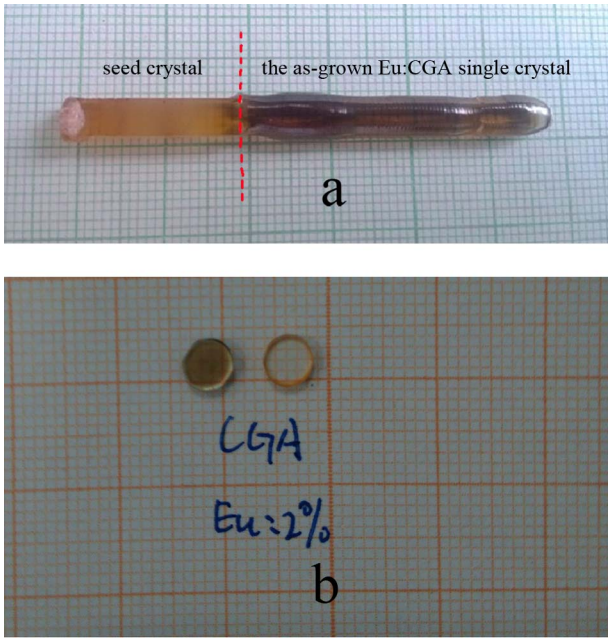

Fig. 1. (a) Photograph of Eu:CGA single crystal grown by the FZ method. (b) Photograph of Eu:CGA obtained slices: the left one is as grown, and the right one is an annealed crystal.

Instruments ACTON 2500i monochromator coupled with a Hamamatsu C5680 streak camera. All spectroscopic measurements were carried out on the annealed samples. All measurements were performed at room temperature. For polarized experiments, a Harrick PGT-S1 V Glan-Tylor polarizer was used.

The XRD patterns of the grown crystal and appropriate Joint Committee On Powder Diffraction Standards (JCPDS) database entry (no. 24-0192) are shown in Fig. 2. The diffraction patterns of the obtained material are in very good agreement with the database record. The cell parameters of the Eu:CGA and pure CGA crystals were calculated from the diffraction data and are listed in Table 1. The calculated parameters for both the doped and pure CGA are quite similar, which is evidence of the integrity of the Eu:CGA structure. The incorporation of dopant ions leads to the extension of the unit cell. This

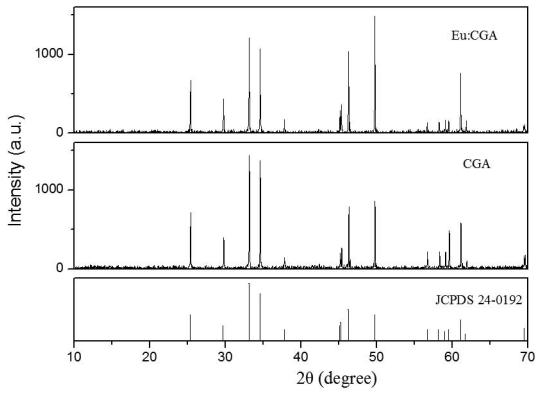

Fig. 2. Powder XRD patterns of Eu:CGA and CGA single crystals grown by the FZ method.

Table 1. Cell Parameters of Eu:CGA and CGA Single Crystals

	A, B (nm)	C (nm)	V (nm^3)
CGA	0.3660	1.1971	0.1604
CGA:Eu	0.3661	1.1986	0.1606

fact can be easily explained: the larger Eu^{3+} ions act as substitutes for the smaller Gd^{3+} ions in the crystal structure ($r_{Eu} = 1.120$ Å, $r_{Gd} = 0.938$ Å). The site occupancy is expected to be determined largely by considerations of ionic size. In consequence, Eu^{3+} ions are expected to preferentially occupy Ca^{2+}/Gd^{3+} sites because the radius of Eu^{3+} (1.120 Å) is closer to those of Ca^{2+} (1.18 Å) and Gd^{3+} (0.938 Å), and is much larger than that of Al^{3+} (0.535 Å). In addition, the similar valency is the other favorable factor to determine the site occupancy, which makes it preferred that the Gd^{3+} ions in the $CaGdAlO_4$ host be replaced by Eu^{3+} ions[25].

The result of the rocking curve for the Eu:CGA crystal is shown in Fig. 3. The only peak indicates that the as-grown crystal is a single crystal. The full width at half-maximum of the rocking curve for the Eu:CGA crystal is about 17 arcsec, which shows the high crystallinity of the crystal grown by the FZ method.

The segregation coefficient of Eu^{3+} in the Eu:CGA crystal can be calculated from the following formula:

$$K_0 = C_s/C_l, \tag{1}$$

where C_s and C_l are the Eu^{3+} concentrations in the crystal and melt, respectively, when there is a solid–liquid equilibrium[20,26]. Approximately, we calculate C_s as the concentration at the growth starting position in the crystal, and C_l as the doping concentration. The element analysis results are listed in Table 2. The segregation coefficient of Eu^{3+} was calculated to be 0.96. The reason is that the radius of Eu^{3+} is larger than the radius of Gd^{3+}, leading to the slight lattice distortion and difficulties in Eu^{3+} replacing the Gd^{3+}. The obtained value of the segregation coefficient suggests that Eu^{3+} should be uniformly distributed along the crystal boule[27].

Table 2. Element Analysis Results From the ICP-AES of the Obtained Eu:CGA Single Crystal

Crystal	Measured (wt. %)	Calculated molar number (at. %)	C_0 (at. %)	Segregation coefficient of Eu^{3+}
Eu:CGA	1.01	1.92	2	0.96

The polarized absorption spectra of Eu:CGA in the range of 300–475 nm are shown in Fig. 4, Both spectra are dominated by a strong line occurring at 399 nm that is related to the $^7F_0 \rightarrow {}^5L_6$ transition. The absorption bands lack a refined structure due to the random crystal environment, which affects the influence of the crystal field on the Eu ions. The Eu ions are located in a site that is randomly occupied by Gd^{3+}; therefore, the Eu ions distributed in a disorderly manner in the Eu:CGA single crystal. All tetragonal crystals are optically uniaxial. For those crystals, the optical axis is parallel to the crystallographic c-axis. The differences between the σ and π polarization absorption spectra reflect the anisotropy of Eu:CGA crystal. The effective absorption coefficients of the $^7F_0 \rightarrow {}^5L_6$ transition at 399 nm for σ polarization and π polarization were calculated to be 3.85 and 7.57 cm^{-1}, the full widths at half-maximum were 1.58 and 1.62 nm, and the absorption cross sections σ_{abs} were calculated to be 1.61×10^{-20} and 3.17×10^{-20} cm^2, respectively.

Figure 5 shows the emission spectra of the Eu:CGA in the region from 500–750 nm under the 399 nm excitation. Some characteristic emission lines correspond to the transitions from the $^5D_0$ excited state to the ground states ^7F_J ($J = 0,\ 1,\ 2,\ 3,\ 4$): $^5D_0 \rightarrow {}^7F_0$ (581 nm), $^5D_0 \rightarrow {}^7F_1$ (591 nm, 599 nm), $^5D_0 \rightarrow {}^7F_2$ (613 nm, 621 nm), $^5D_0 \rightarrow {}^7F_3$ (658 nm), and $^5D_0 \rightarrow {}^7F_4$ (691 nm, 701 nm). Among these emission bands, 621 nm ($^5D_0 \rightarrow {}^7F_2$) is observed to be the most intense. From the emission spectra, we can only find the emission transitions from the $^5D_0$ state to ^7F_J. While the transitions from the ^5D_J to the ^7F_J multiplet are expected in theory, the absence of emissions could be due to the existence of higher energy phonons in the

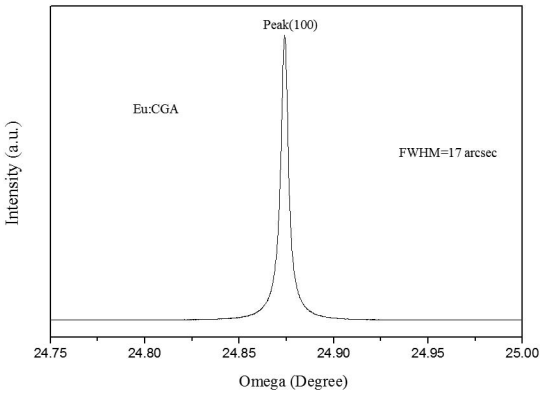

Fig. 3. Result of the rocking curve for the as-grown Eu:CGA single crystal.

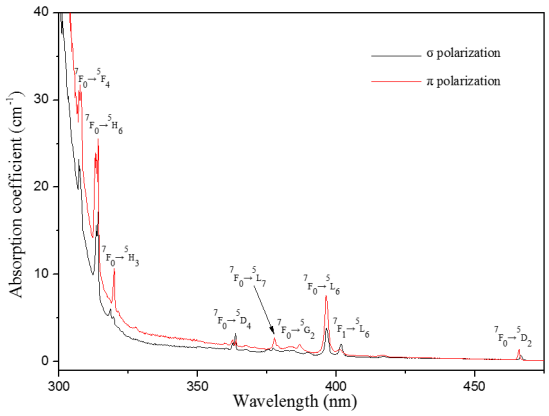

Fig. 4. Polarized absorption spectra of Eu:CGA single crystal at room temperature.

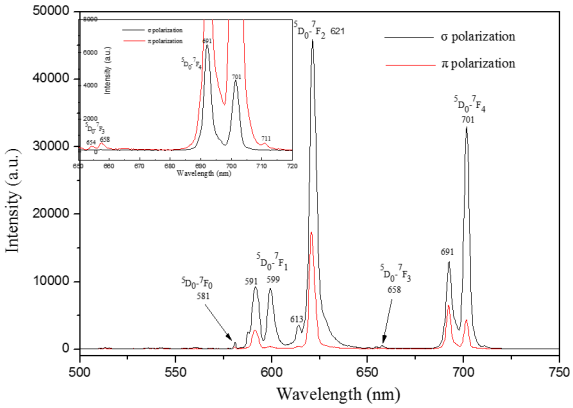

Fig. 5. Emission spectra of Eu:CGA single crystal from 500 to 750 nm.

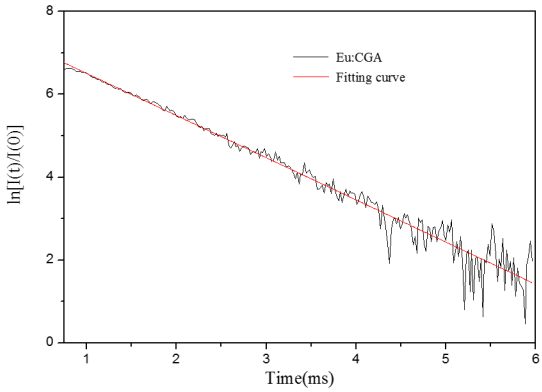

Fig. 6. Decay curves of the Eu:$^5D_0$ level in the Eu:CGA crystal.

CGA, and also could be due to fast nonradiative multiphonon relaxations from these levels to the $^5D_0$ level.

The transition $^5D_0 \rightarrow {}^7F_1$ is a magnetic dipole transition and is allowed with selection rule $\Delta J = \pm 1$ according to the parity selection rules, while the electric dipole emission transition $^5D_0 \rightarrow {}^7F_2$ is forbidden based on selection rule $\Delta J = \pm 2$[13]. If an Eu^{3+} ion occupies a site with inversion symmetry, the orange emission due to the allowed magnetic dipole transition $^5D_0 \rightarrow {}^7F_1$ will be dominant. If it occupies the non-inversion symmetry environment, the $^5D_0 \rightarrow {}^7F_2$ transition is not strictly forbidden, but it is a hypersensitive and forced electric dipole transition. Then, the electric dipole transition $^5D_0 \rightarrow {}^7F_2$ at 621 nm with a bright red emission is dominant. The dominance of the $^5D_0 \rightarrow {}^7F_2$ emission transition at 621 nm suggests that Eu^{3+} is located at a non-inversion symmetry position in CGA, basically agreeing with the random crystal environment of Eu^{3+} ions[28].

Crystal field splitting for rare-earth ions is usually small as compared to the gaps between J multiplets belonging to a definite LJ term, defined as the LSJ terms (Here the L, S, J represent the orbital quantum number, spin quantum number and total angular momentum quantum number respectively)[29]. In this case, the splitting lines observed at the peaks at 591, 621, 658, and 701 nm (shown in Fig. 5) can be attributed to the crystal field spectra of Eu^{3+}. The space group for the $CaGdAlO_4$ tetragonal crystals is I4/mmm. The Ca^{2+} and Gd^{3+} sites have C4v point symmetry. Crystal field splitting for the following lines is expected from the theoretical analysis: $^7F_1$ splits into 2 levels (electric dipole transition and magnetic dipole transition), $^7F_2$ splits into 2 levels (electric dipole transition), $^7F_3$ splits into 2 levels, and $^7F_4$ splits into 4 levels, but we can only find 3 levels at 701 nm, for the other is too weak to see. Only one emission peak at 581 nm corresponding to the $^5D_0 \rightarrow {}^7F_0$ transition was detected, reflecting that the Eu^{3+} ions occupy only one kind of crystallographic site[30], which is also consistent with the results of the cell parameters we calculated in Table 1.

The luminescence decay characteristic of Eu:CGA excited by femtosecond laser pulses ($\lambda_{ex} = 399$ nm) at room temperature is shown in Fig. 6. The decay curve could be well fitted with a single exponential function, $I = I_0 \exp(t/\tau)$ (I_0 is the initial intensity at $t = 0$, and τ represents the 1/e lifetime)[25]. The decay time was calculated to be 1.02 ms, which is a moderate value for oxide materials doped with Eu^{3+} ions such as $CaGd_4O_7$ nanocrystalline phosphors (0.76 ms)[31], tellurite ceramics (0.93 ms)[32], zinc-tellurite glasses (0.98 ms)[33], and $CsZnPO_4$ monophosphate (0.98 ms)[34]. All these results indicate that Eu^{3+} doped in a CGA crystal can be an effective luminescence material.

In conclusion, we successfully grow an Eu:CGA single crystal by the FZ method. The XRD, x ray rocking curve, segregation coefficient, polarized absorption spectra, emission spectra, and luminescence decay kinetics are used to characterize the sample. The result of XRD indicates the structural integrity of the Eu:CGA, and the crystal shows a full width at half-maximum as small as 17 arcsec by the x ray rocking curve measurement. Both results reveal that the single crystal we grow is of high quality. The segregation coefficient is estimated to be 0.96, close to 1, which is helpful in improving the efficiency of the fluorescence. From the spectrum, the f–f transitions of Eu^{3+} in the host lattice are assigned and discussed in detail. The absorption cross sections are calculated to be 1.61×10^{-20} and 3.17×10^{-20} cm^2 at 399 nm for σ polarization and π polarization. Two lines at 599 and 621 nm are observed in the emission spectra of the $^5D_0$–$^7F_1$ and $^5D_0$–$^7F_2$ transitions, and the latter line is much stronger than the former line, which is due to the random crystal environment of Eu^{3+} ions in a CGA single crystal. The decay time of Eu:$^5D_0$ is measured to be 1.02 ms, slightly longer than some other Eu^{3+}-doped media. All the results show that Eu:CGA crystal has good optical characterization and promises to be an excellent red fluorescence material.

This work was supported by the Natural Science Foundation of Shanghai under Grant No. 15ZR1444700.

References

1. M. Gong, W. Xiang, X. Liang, J. Zhong, D. Chen, J. Huang, G. Gu, C. Yang, and R. Xiang, J. Alloys Compd. **639**, 611 (2015).

2. Y. Zhang, X. Li, K. Li, H. Lian, M. Shang, and J. Lin, ACS Appl. Mater. Interfaces **7**, 2715 (2015).
3. B. Yu, H. Zhang, and H. Dong, Chin. Opt. Lett. **12**, 110606 (2014).
4. L. Mengting and J. Baoxiang, J. Rare Earths **33**, 231 (2015).
5. F. Kang, M. Peng, Q. Zhang, and J. Qiu, Chem. Eur. J. **20**, 11522 (2014).
6. F. Kang, Y. Zhang, and M. Peng, Inorg. Chem. **54**, 1462 (2015).
7. F. Kang, X. Yang, M. Peng, L. Wondraczek, Z. Ma, Q. Zhang, and J. Qiu, J. Phys. Chem. C **118**, 7515 (2014).
8. Y. Jiang, H. Xia, S. Yang, J. Zhang, D. Jiang, C. Wang, and B. Chen, Chin. Opt. Lett. **13**, 071601 (2015).
9. B. M. Tissue and H. B. Yuan, J. Solid State Chem. **171**, 12 (2003).
10. Y. Wu, X. Xu, X. Yu, B. Zhang, Q. Li, and J. Qiu, Chin. Opt. Lett. **12**, 101602 (2014).
11. M. H. V. Werts, R. T. F. Jukes, and J. W. Verhoeven, Phys. Chem. Chem. Phys. **4**, 1542 (2002).
12. N. Kodama and M. Yamaga, Phys. Rev. B **57**, 811 (1998).
13. L. Zhou, J. Shi, and M. Gong, J. Rare Earths **24**, 138 (2006).
14. X. Li, Y. Zhang, D. Geng, J. Lian, G. Zhang, Z. Hou, and J. Lin, J. Mater. Chem. C **2**, 9924 (2014).
15. N. Kodama and M. Yamaga, Phys. Rev. B **57**, 811 (1998).
16. A. Agnesi, A. Greborio, F. Pirzio, G. Reali, J. Aus der Au, and A. Guandalini, Opt. Express **20**, 10077 (2012).
17. J. Boudeile, F. Druon, M. Hanna, P. Georges, Y. Zaouter, E. Cormier, J. Petit, P. Goldner, and B. Viana, Opt. Lett. **32**, 1962 (2007).
18. A. A. Lagatskii, N. V. Kuleshov, V. G. Shcherbitskii, V. F. Kleptsyn, V. P. Mikhailov, V. G. Ostroumov, and G. Huber, Quantum Electron. **27**, 15 (1997).
19. J. H. Huang, X. H. Gong, Y. J. Chen, Y. F. Lin, Z. D. Luo, and Y. D. Huang, J. Alloys Compd. **585**, 163 (2014).
20. J. Di, X. Xu, C. Xia, Q. Sai, D. Zhou, Z. Lv, and J. Xu, J. Lumin. **155**, 101 (2014).
21. C. R. Phillips, A. S. Mayer, A. Klenner, and U. Keller, Opt. Express **22**, 5913 (2014).
22. D. Z. Li, X. D. Xu, J. Zhang, Z. H. Cong, D. Y. Tang, J. Ma, H. M. Zhu, X. Y. Chen, F. Wu, C. T. Xia, and J. Xu, Laser Phys. Lett. **8**, 647 (2011).
23. Z. Chen, Y. Hang, X. Wang, and J. Wang, Opt. Mater. **46**, 12 (2015).
24. R. Saint-Martin, P. Berthet, and A. Revcolevschi, J. Cryst. Growth **415**, 118 (2015).
25. D. Geng, G. Li, M. Shang, C. Peng, Y. Zhang, Z. Cheng, and J. Lin, Dalton Trans. **41**, 3078 (2012).
26. C. Yan, G. Zhao, L. Su, X. Xu, L. Zhang, and J. Xu, J. Phy.: Condens. Matter **18**, 1325 (2006).
27. Z. Jia, X. Tao, H. Yu, C. Dong, J. Zhang, H. Zhang, Z. Wang, and M. Jiang, Opt. Mater. **31**, 346 (2008).
28. V. Naresh, B. H. Rudramadevi, and S. Buddhudu, J. Alloys Compd. **632**, 59 (2015).
29. F. Kang, Y. Hu, L. Chen, X. Wang, Z. Mu, H. Wu, and G. Ju, Appl. Phys. B. **107**, 833 (2012).
30. L. Zhou, J. Shi, and M. Gong, J. Rare Earths **24**, 138 (2006).
31. E. Pavitra, G. S. R. Raju, J. Y. Park, Y. H. Ko, and J. S. Yu, J. Alloys Compd. **553**, 291 (2013).
32. W. Stambouli, H. Elhouichet, B. Gelloz, and M. Férid, J. Lumin. **138**, 201 (2013).
33. S. S. Babu, K. Jang, E. J. Cho, H. Lee, and C. K. Jayasankar, J. Phys. D: Appl. Phys. **40**, 5767 (2007).
34. R. Yu, H. Li, H. Ma, C. Wang, and H. Wang, Solid State Sci. **29**, 34 (2014).